Nonlinear Dyn (2014) 78:1629–1643
DOI 10.1007/s11071-014-1546-3

ORIGINAL PAPER

A pseudo-stable structure in a completely invertible bouncer system

Mantas Landauskas · Minvydas Ragulskis

Received: 8 October 2013 / Accepted: 15 June 2014 / Published online: 2 July 2014

Abstract It is shown that a pseudo-stable structure of non-asymptotic convergence may exist in a completely invertible bouncing ball model. Visualization of the pattern of H-ranks helps to identify this structure. It appears that this structure is similar to the stable manifold of non-invertible nonlinear maps which govern the non-asymptotic convergence to unstable periodic orbits. But this convergence to the unstable repeller of the bouncing ball problem is only temporary since non-asymptotic convergence cannot exist in completely invertible maps. This nonlinear effect is exploited for temporary stabilization of unstable periodic orbits in completely reversible nonlinear maps.

Keywords Bouncing ball model · Rank · Manifold · Convergence

1 Introduction

A particle falling down, in a constant gravitational field, on a moving platform is called a bouncing ball problem, or a bouncer. This model was suggested more than thirty years ago [28,31] as an alternative simplification to the Fermi–Ulam model [22] of cosmic ray acceleration [5]. Many different approaches to the bouncer model have been studied theoretically and experimentally [2,4,21,27]. It has been proved to be a useful model for experimental exploration of several new nonlinear effects [8,17,24,30]. Moreover, it has been implemented into a number of engineering applications [12,13,23].

The bouncer model is a discrete dynamical system, since the time evolution of the dynamics of the system is discontinuous at collisions. The bouncer model can be briefly characterized by the following basic statements: (i) Maps derived for the bouncer model can be exactly iterated for any number of iterations into the future [27,30]. (ii) The ball-platform collisions can be characterized by a coefficient of restitution α changing from $\alpha = 1$ for a perfectly elastic case to $\alpha = 0$ for a completely inelastic situation. (iii) The chaotic bouncer can be easily used to relate theoretical predictions to experimental results, [17,30] what makes it a paradigmatic model in nonlinear dynamics.

The bouncer model is a discrete dynamical system, since the time evolution of the dynamics of the system is discontinuous at collisions. If the impact between the table and the ball is inelastic, we can represent the velocity of the ball just after the impact with the help of a discrete map which is called the bouncer system [7,11,15]

M. Landauskas (✉)
Research Group for Mathematical and Numerical Analysis of Dynamical Systems, Kaunas University of Technology, Studentu 50-146, LT-51368 Kaunas, Lithuania
e-mail: mantas.landauskas@ktu.lt

M. Ragulskis
Research Group for Mathematical and Numerical Analysis of Dynamical Systems, Kaunas University of Technology, Studentu 50-147, LT-51368 Kaunas, Lithuania
e-mail: minvydas.ragulskis@ktu.lt

$$\begin{cases} x_{n+1} = x_n + y_n; \\ y_{n+1} = \alpha y_n + \beta cos\,(x_n + y_n)\,, \end{cases} \tag{1}$$

where the variable x_n is the time interval between the $(n-1)$th and the nth collisions of the ball and y_n is the velocity of the ball immediately after the nth impact. The parameter $\alpha \in (0, 1]$ is the coefficient of restitution and the parameter β is associated with the table frequency. If the coefficient of restitution is $\alpha = 1$, then Eq. (1) reduces to the standard map. Note that the bouncer system described by Eq. (1) is a good approximation of the bouncing ball [8].

The knowledge of the stable and unstable manifolds of hyperbolic equilibria plays a central role in understanding many global, dynamical issues for autonomous maps. For a given nonlinear dynamical system, the only general way of studying such stable and unstable manifolds is by computing them numerically. Consequently, a number of different algorithms have been developed for computing the stable and unstable manifolds for autonomous maps [1,3,6,10,16,18,25,26].

Unstable periodic orbits in nonlinear maps can be identified by clocking the convergence processes. A pattern of H-ranks (which does help to clock the convergence) is a particularly useful tool for the visualization of these unstable orbits and their manifolds in non-invertible nonlinear maps [19]. But a non-asymptotic convergence to an unstable orbit cannot exist in a completely invertible map (this statement can be easily proven by the contradiction). Nevertheless, a "shadow" of a previously stable orbit (after a period doubling bifurcation) will still temporarily attract transient processes from some initial conditions in a completely invertible bouncing ball model. The question that how to identify these "shadows" for an unstable orbit for a completely invertible map remains open.

We use computational tools based on H-ranks [19,29] for the assessment of the convergence rate to stable periodic orbits of the bouncer model. The resulting patterns of H-ranks reveal interesting structures in the phase space of initial conditions. The fact that "shadows" of unstable orbits can be interpreted in these patterns of H-ranks is not unexpected. Much more interesting is the topological structure of these "shadows" which appears to be strikingly similar to the stable manifold of a non-invertible one-dimensional logistic map and suggests the existence of the non-asymptotic temporary convergence to the unstable repeller. The main objective of this paper is to demonstrate the existence of this non-asymptotic convergence and its ability to stabilize unstable periodic orbits of discrete completely invertible dynamical systems during finite transient processes.

2 Preliminaries

Period-1 fixed points of the bouncer model can be easily determined by setting $x_{n+1} = x_n$ and $y_{n+1} = y_n$ into Eq. (1). Two different fixed points exist: $x^{(1)} = \frac{\pi}{2} + 2\pi k$; $y^{(1)} = 0$ and $x^{(2)} = -\frac{\pi}{2} + 2\pi k$; $y^{(2)} = 0$; $k \in Z$. The stability of these points can be determined by evaluating the eigenvalues of the Jacobian matrix; corresponding eigenvalues read:

$$\lambda_{1,2}\left(x^{(k)}, y^{(k)}\right) = \frac{1}{2}\left(1 + \alpha - \beta \sin x^{(k)}\right) \pm \frac{1}{2}\sqrt{(1-\alpha)^2 - 2\,(1+\alpha)\,\beta \sin x^{(k)} + \beta^2 \sin^2 x^{(k)}}; \quad k = 1, 2.$$

We fix $\alpha = 0.1$ and explore the variation of eigenvalues in respect to β:

$$\lambda_{1,2}\left(x^{(1)}, y^{(1)}\right) = \frac{(1.1-\beta) \pm \sqrt{0.81 - 2.2\beta + \beta^2}}{2},$$

$$\lambda_{1,2}\left(x^{(2)}, y^{(2)}\right) = \frac{(1.1+\beta) \pm \sqrt{0.81 + 2.2\beta + \beta^2}}{2}.$$

The values of $\lambda_{1,2}\left(x^{(k)}, y^{(k)}\right)$; $k = 1, 2$ are plotted in Fig. 1. It can be seen that the fixed point $\left(x^{(1)}, y^{(1)}\right)$ is stable in the interval $0 < \beta < 2.200$ (both absolute values of its eigenvalues are lower than 1) and its stability is lost as β exceeds 2.200 (Fig. 1a). This fact can be observed in the bifurcation diagram (Fig. 2), where the first period doubling bifurcation occurs at $\beta = 2.200$.

3 Patterns of H-ranks

3.1 The H-rank of a sequence—preliminaries

The H-rank of a sequence is an effective computational tool for the investigation of the convergence of nonlinear dynamical systems to critical attractors. H-ranks computed for initial solutions in the space of system's parameters and initial conditions may reveal important physical information about peculiarities of system's behavior [19,29].

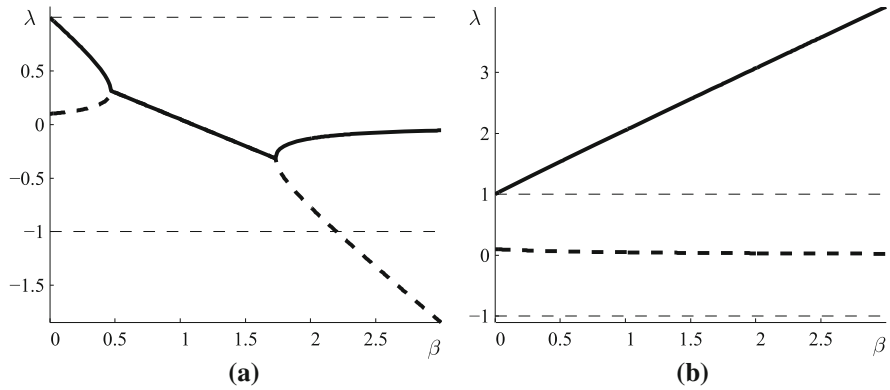

Fig. 1 The eigenvalues of the Jacobian for $\left(x^{(1)}, y^{(1)}\right)$ (part **a**) and $\left(x^{(2)}, y^{(2)}\right)$ (part **b**)

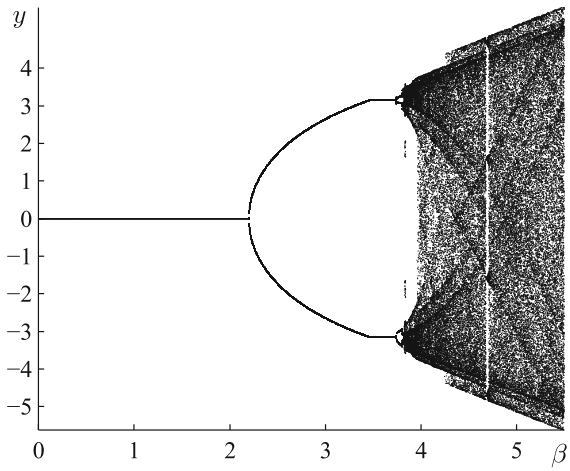

Fig. 2 The bifurcation diagram for the bouncer model; $\alpha = 0.1$

Let S is an infinite sequence of real or complex numbers: $S := \{x_r\}_{r=0}^{+\infty}$.

A finite subsequence comprising first $2k-1$ elements $(x_0, x_1, x_2, \ldots, x_{2k-3}, x_{2k-2})$ can be rearranged into the Hankel matrix $H^{(k)}$:

$$H^{(k)} := \left[x_{r+s-2}\right]_{1\le r,s\le k} = \begin{bmatrix} x_0 & x_1 & \cdots & x_{k-1} \\ x_1 & x_2 & \cdots & x_k \\ & & \cdots & \\ x_{k-1} & x_k & \cdots & x_{2k-2} \end{bmatrix}$$

where the superscript k denotes the order of the Hankel matrix. The Hankel transform of the sequence of matrices $\left\{H^{(k)}\right\}_{k=2}^{+\infty}$ yields a sequence of determinants $\left\{\det\left(H^{(k)}\right)\right\}_{k=2}^{+\infty} = \left\{d^{(k)}\right\}_{k=2}^{+\infty}$.

The rank of a discrete sequence is defined in [29]. It is such a natural number m that satisfies the following condition (if only the rank exists): $d^{(m+n)} = 0$ for all $n \in N$; if only $d^{(m)} \neq 0$. We will use the notation:

$$HrS = m.$$

If such a number m does not exist, we will denote that the sequence S does not have a rank: $HrS := +\infty$. But if the rank of a discrete sequence does exist, an explicit mathematical model governing the evolution of that sequence can be derived [29].

It can be noted that a chaotic sequence does not have a rank. Otherwise, the dynamics of that sequence would be deterministic because an algebraic model of this sequence could be derived, which contradicts to the definition of a chaotic sequence.

3.2 Patterns of H-ranks for the bouncer model

Patterns of H-ranks for the bouncer model produced at different values of the parameter β are illustrated in Fig. 3. Every point in the phase space $(x_0; y_0)$ corresponds to a separate transient process started from initial conditions $(x_0; y_0)$. The color of a point is assigned in accordance to the H-rank of a transient process started from this point. But H-ranks can be computed for scalar time series only [29]. Therefore, we compute $Hr\left(\sqrt{x_0^2+y_0^2}, \sqrt{x_1^2+y_1^2}, \sqrt{x_2^2+y_2^2}, \ldots\right)$ for a particular trajectory in the two-dimensional phase plane. Such an approach ensures the consistency of results and eliminates the possibility for the recovery of low H-ranks for such transient processes where one coordinate is frozen and the other performs wild oscillations.

The computation of the H-rank of a transient process for a predefined set of system parameters and initial conditions can be described by the following algorithm. Step 0: Set the maximum dimension $\overline{m}$ of the square Hankel matrix; set $\varepsilon > 0$. Step 1: Compute the Hankel transform of the transient process up to $k = \overline{m}$ resulting into a sequence of determinants $\{d_k\}_{k=2}^{\overline{m}}$. Step 2: Find

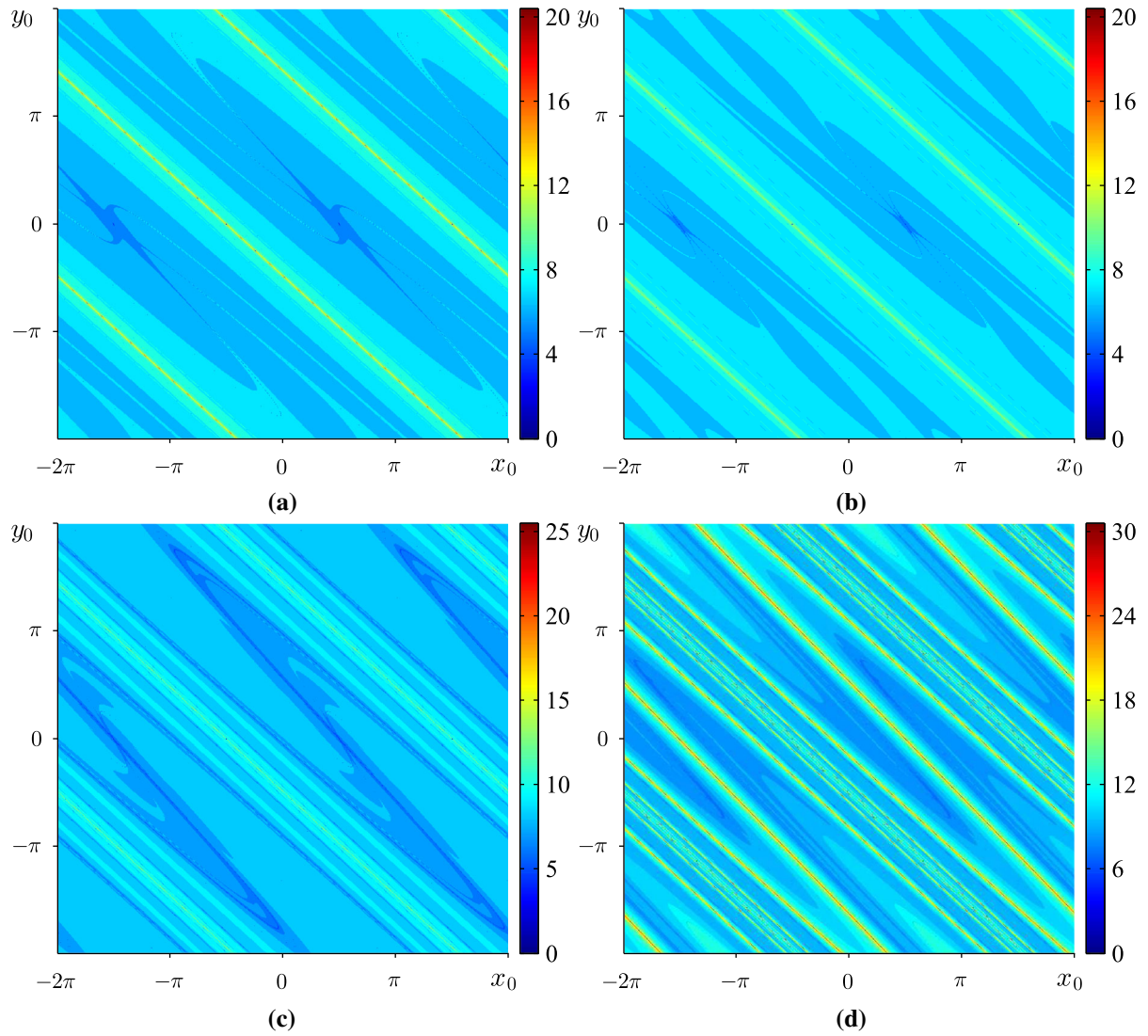

Fig. 3 Patterns of H-ranks computed for the bouncing ball model at different values of β: **a** $\beta = 1$; **b** $\beta = 1.5$; **c** $\beta = 2$; **d** $\beta = 2.5$. The parameter α is fixed to 0.1; all computations are performed in the region ($-2\pi \leq x_0 \leq 2\pi$ and $-2\pi \leq y_0 \leq 2\pi$)

such $2 \leq s \leq \overline{m}$ that $\{|d_k|\}_{k \geq s+1}^{\overline{m}} < \varepsilon$; assign the H-rank of the sequence to s. If $|d_{\overline{m}}| \geq \varepsilon$ then assume that the H-rank is greater or equal than $\overline{m}$.

Detailed description of computational properties of this algorithm, and more efficient realizations based on SVD and PLU decompositions are investigated in [20].

Several characteristic features can be singled out in all patterns of H-ranks illustrated in Fig. 3. All patterns of H-ranks are periodic in respect to x_0 (due to the periodical structure of the model in respect of x). Stable period-1 attractors are clearly visible at $x_0 = \frac{\pi}{2} + 2\pi k$; $y_0 = 0$; $k \in N$ in Fig. 3a–c (period-1 orbit is unstable in Fig. 3d). Also, it can be noted that the boundary lines separating periodic bands of patterns run through unstable period-1 fixed points ($x_0 = -\frac{\pi}{2} + 2\pi k$; $y_0 = 0$; $k \in N$) in all figures, including Fig. 3d.

3.3 Visualization of patterns of H-ranks in sheared bands

It would be advantageous to visualize the pattern of H-ranks in one single periodic band. A straightforward parallel plain shear mapping could be used for such

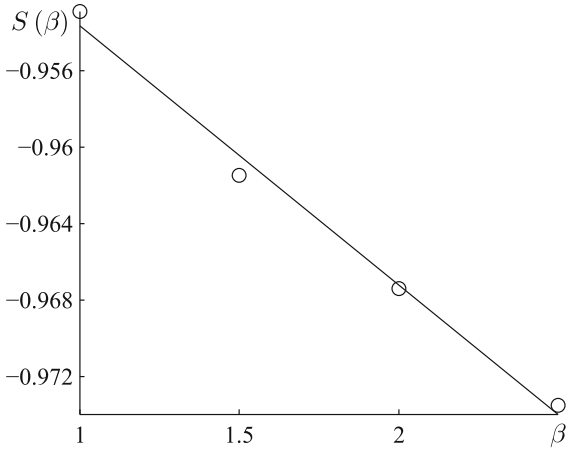

Fig. 4 Numerical reconstruction of the slope of separatrices S(β). *Circles* denote numerically reconstructed values of the slope at $\beta = 1$; 1.5; 2; and 2.5; the *solid line* represents the least squares linear approximation of S(β)

visualization. Unfortunately, the slope of lines separating adjacent bands is different for different β (Fig. 3). We use numerical techniques for the approximation of the slope of separatrices (at fixed $\alpha = 0.1$):

$$y = -S(\beta) \cdot \left(x + \frac{\pi}{2} + 2\pi k\right); k \in N.$$

Numerical values of the parameter $S(\beta)$ are reconstructed from the results of numerical experiments: $S(1) = -0.9529$; $S(1.5) = -0.9615$; $S(2) = -0.9674$; $S(2.5) = -0.9735$. The least square linear regression yields the approximation (Fig. 4):

$$S(\beta) = -0.01354 \cdot \beta - 0.94013;$$

Now, the plain shear mapping reads

$$x := x + \frac{y}{S(\beta)};$$
$$y := y.$$

This mapping is used to visualize only one band between two adjacent separatrices; both separatrices are represented as vertical border lines on the left and the right side of the mapped image of H-ranks (Fig. 5). Note that all mapped coordinates at $y_0 = 0$ correspond to the original coordinate system—stable fixed points are located $x_0 = \frac{\pi}{2}$; $y_0 = 0$ at Fig. 5a–c. Two period-2 fixed points are clearly visible in Fig. 5d (they are located in the centers of regions represented by the lowest H-rank). Note that period-2 fixed points are separated by a new separatrix; this separatrix does cross the previously stable period-1 point at $x_0 = \frac{\pi}{2}$; $y_0 = 0$ (Fig. 5d).

3.4 The continuous variation of β

Snapshots of patterns of H-ranks in Figs. 3 and 5 are illustrated at four discrete values of the parameter β. Continuous variation of the parameter β would help to reveal the evolution of these patterns of H-ranks. In order to simplify the graphical data representation, we cut every pattern in Fig. 5 in the vertical and the horizontal direction through the point $\left(x_0 = \frac{\pi}{2}; y_0 = 0\right)$. The resulting graphs (as β varies continuously from 0 to 4) are shown in Fig. 6b (the vertical cut) and Fig. 6a (the horizontal cut).

The pattern of H-ranks in Fig. 6b reveals the period doubling bifurcation occurring at $\beta = 2.200$. The fixed point $\left(x_0 = \frac{\pi}{2}; y_0 = 0\right)$ becomes unstable after the first period doubling bifurcation; a characteristic supercritical pitchfork shape can be observed in Fig. 6b after the bifurcation point. Note that the outer pitchfork fingers do not represent the stable period-2 solution in Fig. 6b— the vertical cutting line does not intersect the stable period-2 attractor (Fig. 5d).

The unstable finger of the pitchfork is surrounded by a region of high H-ranks after the period doubling bifurcation (Fig. 6b). That represents the transient behavior of solutions with initial conditions in the vicinity of the unstable period-1 fixed point. The system would be repelled to the stable period-2 attractor at $\beta = 2.5$. But this repelling process is slow if initial conditions are very close to the unstable period-1 fixed point (the "shadow" of the previously stable attractor is still there [9]). The pattern of H-ranks surrounding the unstable period-1 repeller forms a shape of a tulip. Such ornament represents the fact that the algebraic complexity of the transient process from initial conditions near the repeller is high—the system starts slowly moving away from the unstable period-1 attractor and subsequently converges (after a rather long transient time) to the stable period-2 attractor.

4 Non-asymptotic temporary convergence

Let us consider the evolution of the pattern in H-ranks in vertical sections (Fig. 6a). The supercritical pitchfork of the period doubling bifurcation is also visible at $\beta = 2.200$. But one can observe a rather interesting structure of patterns in the region after the first period doubling bifurcation. Such structures in the pattern of H-ranks require additional attention.

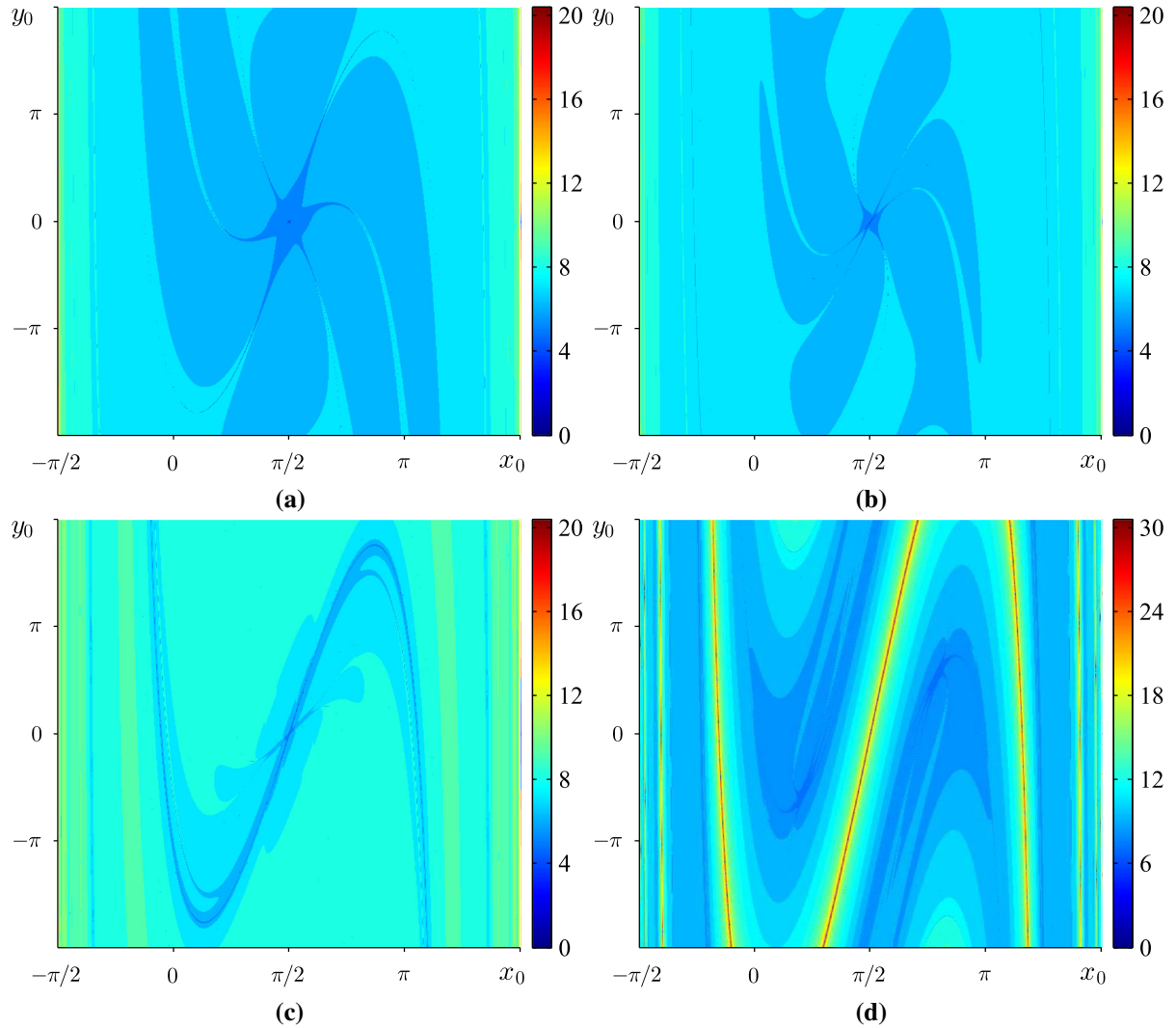

Fig. 5 Patterns of H-ranks in a periodic sheared band computed at different values of β: **a** $\beta = 1$; **b** $\beta = 1.5$; **c** $\beta = 2$; **d** $\beta = 2.5$. The parameter α is fixed to 0.1

4.1 The stable manifold of the bouncer model

We exploit Dynamics [26] software for the construction of the stable and unstable manifolds of the bouncer model. The stable and the unstable manifolds of the bouncer model are illustrated in Fig. 7 at $\alpha = 0.1$ and $\beta = 2.5$.

4.2 The pseudo-stable structure of the bouncer model

Let us consider the pattern of H-ranks constructed for the continuous variation of β in horizontal sections (Fig. 6b). A vertical band of H-ranks around $\beta = 2.5$ is illustrated in Fig. 8a. Let us denote the region of higher H-ranks wrapped around the central line $x_0 = \frac{\pi}{2}$ as the central tulip. Regions of higher H-ranks above and below the central line are denoted as the first upper and the first lower tulip accordingly (marker 2 is located near the first upper tulip in Fig. 8a). Analogously, tulips located further away from the central line are given higher numbers (marker 1 is located at the center of the second upper tulip in Fig. 8a).

It can be observed that initial conditions corresponding to the centers of tulips result into transient processes approaching the unstable period-1 regime and con-

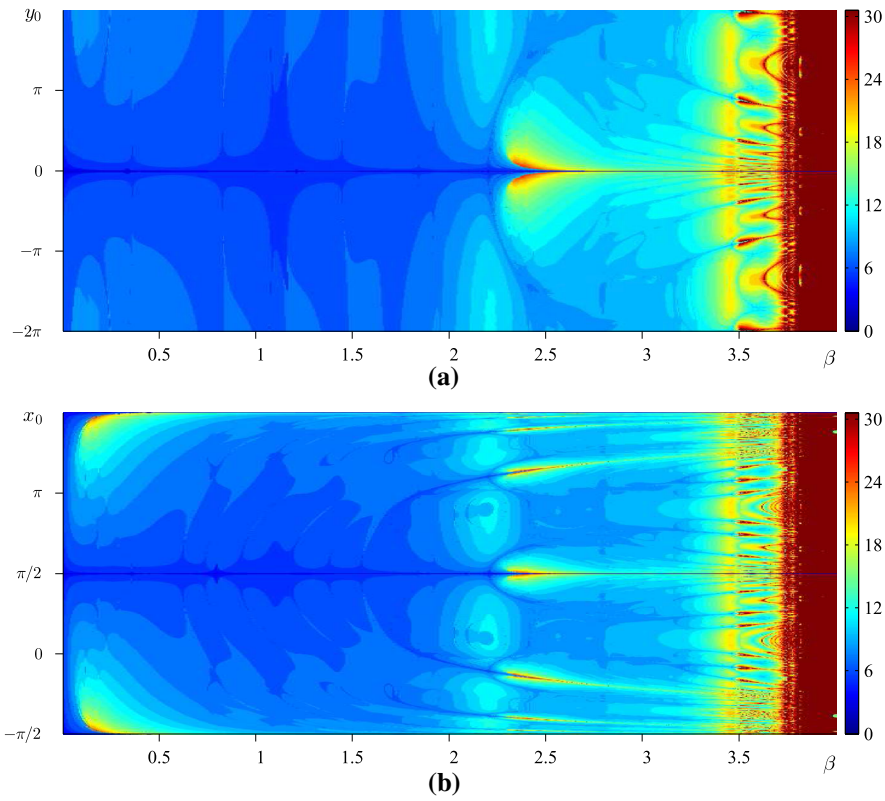

Fig. 6 The evolution of the pattern of H-ranks for the continuous variation of β in horizontal (**a**) and vertical (**b**) sections of sheared bands of H-ranks; the parameter α is fixed to 0.1

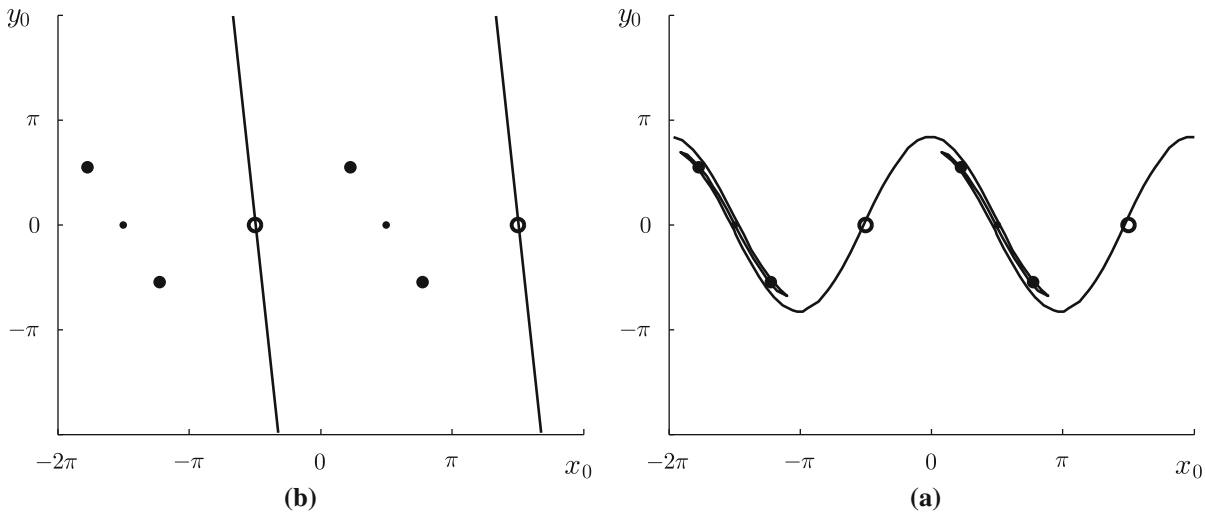

Fig. 7 The stable (**a**) and the unstable (**b**) manifolds of the bouncer model at $\alpha = 0.1$ and $\beta = 2.5$. Saddle points are shown as empty *circles*; stable period-2 points are shown as *black disks*; "shadows" of previously stable period-1 points are shown as *black dots* and are located between each pair of *black disks*. The unstable manifold goes through all equilibrium points (stable and unstable)

sequently converging to the stable period-2 regime (Fig. 8). Initial conditions for the computation experiment illustrated in Fig. 8a are $x_1 = 4.4082$; $y_1 = 0$. Note that y_1 must be equal to zero because the horizontal section though the pattern of H-ranks in Fig. 7b is performed through the point $\left(x_0 = \frac{\pi}{2}; y_0 = 0\right)$. Four

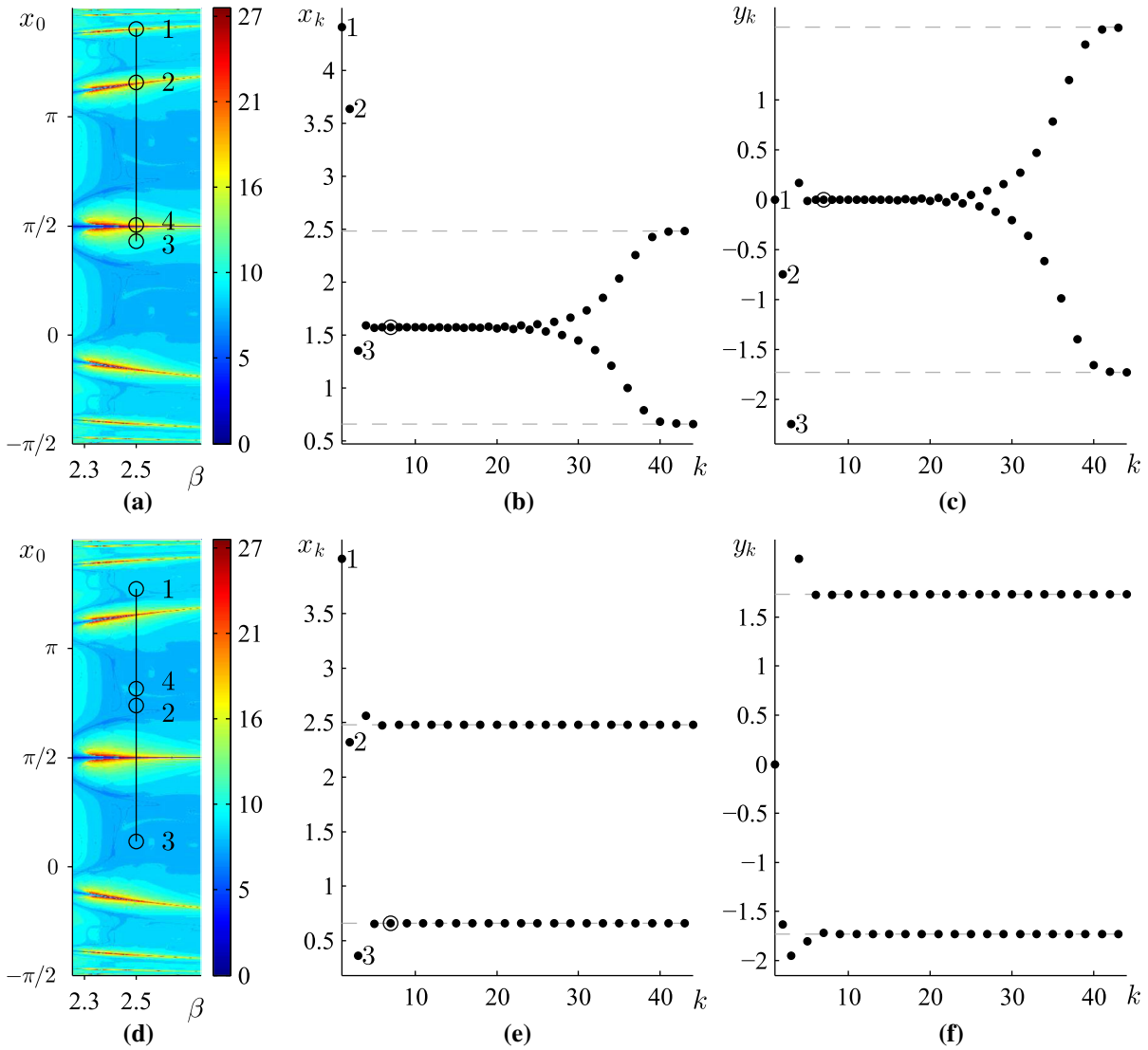

Fig. 8 The evolution of a transient process started from initial conditions coinciding with the center of the second upper tulip in the pattern of H-ranks. Part **a** shows a vertical band of the pattern of H-ranks in Fig. 6b around $\beta = 2.5$; part **b** illustrates the evolution of x_k; part **c**—the evolution of y_k (k is the step number). Initial conditions are marked by the symbol 1 in parts (**a**), (**b**), and (**c**). 4 consecutive steps are illustrated in part (**a**); 44 forward steps are illustrated in parts (**b**) and (**c**). Initial conditions located not in the center of a tulip result into fast convergence to the stable period-2 attractor (parts **d** and **f**). Parameter α is fixed to 0.1; β—to 0.25

consecutive steps of the transient process are illustrated in Fig. 8a, but only x-coordinates are shown there. For example, the coordinates of the second point are $x_2 = 3.6392$; $y_2 = -0.7489$. Therefore, the coincidence of the second point with the center of the first upper tulip in Fig. 8a is completely accidental. The transient process started from the center of the first upper tulip would be different from the process illustrated in Fig. 8 (though it would also approach the unstable period-1 regime and then converge to the stable period-2 regime).

The evolution of x_k and y_k is illustrated in Fig. 8b and c. The transient process approaches the unstable period-1 fixed point $\left(x_0 = \frac{\pi}{2};\ y_0 = 0\right)$ but never reaches it. Empty circles at $k = 6$ in Fig. 8b and c denote the sixth iteration when the system is located closest to this fixed

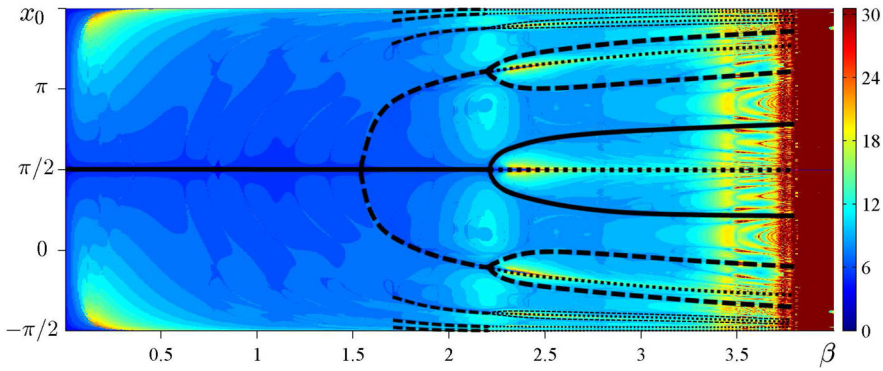

Fig. 9 The schematic diagram illustrating the skeleton-type structure of the pattern of H-ranks. *Thick solid lines* correspond to stable period-1 and period-2 regimes; the *central thick dotted line* corresponds to the unstable period-1 regime. All other *thick dotted lines* belong to the pseudo-stable structure of the unstable period-1 regime

point:

$$\sqrt{\left(x_6 - \frac{\pi}{2}\right)^2 + y_6^2} = 6.8454 \cdot 10^{-8}.$$

As mentioned previously, such temporary convergence to a "shadow" of a previously stable fixed point is not a new phenomenon. But the basin of attraction of this "shadow" is rather unexpected. A schematic diagram drawn on top of Fig. 6a illustrates the complexity of this region (Fig. 9).

The thick solid line in the region $0 < \beta < 2.200$ represents the stable period-1 attractor. The period doubling bifurcation occurs at $\beta = 2.200$; a stable period-2 regime exists at $2.200 < \beta < 3.736$ (we do not visualize the second period doubling bifurcation). The "shadow" of the previously stable period-1 regime is shown as a thick dotted line at $x_0 = \frac{\pi}{2}$. Thick dashed lines before the first period doubling bifurcation correspond to such initial conditions which yield fast convergence to the stable period-1 regime. Analogously, thick dashed lines after the first period doubling bifurcation correspond to such initial conditions which yield fast convergence to the stable period-2 orbit. Finally, thick dotted lines running through the centers of the top and the bottom tulips correspond to such initial conditions which yield fast (though temporary) convergence to the unstable period-1 regime.

It is well known that the bouncer model is a completely invertible discrete nonlinear map; a backward step can be expressed from Eq. (1):

$$\begin{cases} y_{n-1} = \frac{1}{\alpha}\,(y_n - \beta \cos x_n); \\ x_{n-1} = x_n - y_{n-1}. \end{cases}$$

In other words, a unique backward trajectory can be constructed for every initial condition of the bouncer model. That is contrary to discrete non-invertible maps where the process of the convergence to a stable attractor of a nonlinear discrete map can be classified into the asymptotic convergence and the non-asymptotic convergence. An infinite number of forward steps are required for the system to reach the stable attractor if it converges asymptotically. On the opposite, a finite number of forward steps are required to reach the stable attractor if the system converges non-asymptotically. Such different types of convergence to stable attractors of the non-invertible logistic map are well known; some computations aspects for the identification of the type of the convergence are discussed in [29].

But the non-asymptotic convergence cannot exist in the bouncer model. This statement can be proven by contradiction. Let us denote the coordinates of the period-p orbit as $\{(\hat{x}_1; \hat{y}_1), (\hat{x}_2; \hat{y}_2), \ldots, (\hat{x}_p; \hat{y}_p)\}$. Let us assume that the set of initial conditions which yield the convergence to this periodic orbit in a finite number of forward iterations is not an empty set. Then, there exists at least one point $(\hat{x}_0; \hat{y}_0)$ which does not belong to the periodic orbit and is mapped into a point $(\hat{x}_k; \hat{y}_k)$; $1 \le k \le p$ in one forward iteration (otherwise non-asymptotic convergence would be not possible). But then the point $(\hat{x}_k; \hat{y}_k)$ is a branching point—it can be mapped either into the previous point of the orbit $(\hat{x}_{k-1}; \hat{y}_{k-1})$, or into $(\hat{x}_0; \hat{y}_0)$ in one backward iteration. That contradicts to the fact that the bouncer model is a completely invertible discrete map.

4.3 Non-asymptotic convergence and the logistic map

It is well known that the one-dimensional logistic map

$$x_{k+1} = r x_k (1 - x_k); \quad (2)$$

$0 \le r \le 4$; $0 \le x_0 \le 1$; $k = 0, 1, 2, \ldots$ is a non-invertible map. Let us consider a stable period-2 orbit at $r = 3.2$. All initial conditions can be classified into 3 distinct sets: the infinite uncountable set of initial conditions leading to the asymptotic convergence to the period-2 attractor; the infinite countable set of initial conditions leading to the non-asymptotic convergence to the period-2 attractor; and the infinite countable set of initial conditions leading to the non-asymptotic convergence to the unstable period-1 repeller. All three different types of convergence are illustrated in Fig. 10.

But the topological structure of patterns of H-ranks in Figs. 9 and 10 is strikingly similar. As discussed previously, non-asymptotic convergence to stable or unstable attractors is impossible for completely invertible maps. Therefore, initial conditions coinciding with the centers of tulips in the pattern of H-ranks for the bouncer model do not result into a non-asymptotic convergence to the unstable period-1 attractor in Fig. 8 (contrary to the non-invertible logistic map in Fig. 10). The system is just temporarily attracted to the vicinity of the unstable attractor (Fig. 8). Therefore, the topological structure highlighted in Fig. 9 cannot be identified by Dynamics. But this structure does attract (although temporarily) the system to the unstable attractor. Moreover, this attraction reminds a non-asymptotic convergence—the system approaches the unstable attractor in a finite number of forward iterations. Thus, we denote this topological structure as the pseudo-stable structure of the unstable orbit.

5 Temporary stabilization of the unstable period-1 attractor

The ability of the bouncer model to attract transient processes into the vicinity of the unstable attractor can be successfully exploited for the temporary stabilization of unstable orbits. A continuous feedback control loop is not necessary in such case—one can exploit small external pulse which could relocate the system onto a branch of the pseudo-stable structure.

Such a control strategy is illustrated in Figs. 11 and 12. A single impulse relocates the system onto a nearest point lying on the pseudo-stable structure. The system then converges non-asymptotically to the vicinity of the period-1 repeller and stays there for considerable number of forward iterations.

The presented technique for the temporary stabilization of unstable orbits comprises the following steps:

(i) Compute the pattern of H-ranks for the completely invertible discrete map.
(ii) Identify the structure of non-asymptotic pseudo-convergence to unstable orbit in the pattern of H-ranks. Note that non-asymptotic convergence is not possible in a completely invertible discrete map; negative mapping cannot reveal this structure.
(iii) Use a control impulse to reset the system from its current point to the closest branch of this structure of non-asymptotic pseudo-convergence.
(iv) Allow the system to converge (non-asymptotically) to the infinitesimal surrounding of the unstable orbit. Such process of convergence is named as temporary convergence because the system cannot converge exactly to this unstable orbit—otherwise, this system would not be invertible.
(v) The unstable orbit is a repeller—finally the system will diverge from the infinitesimal surrounding of the unstable orbit. But the system will stay in the surrounding of this unstable orbit for a period of time before it converges (asymptotically) to a different stable attractor.

The whole process is named as non-asymptotic temporary convergence to unstable orbits in the completely invertible discrete dynamical system.

6 The sensitivity of the temporary stabilization technique to external noise

The experimental bouncing ball problem is an analog system and computational simulation of this system does introduce numerical noise. We do not only simulate the system, but also compute H-ranks of transient solutions—that introduces additional computational errors. This raises the question about the robustness of the proposed temporary stabilization technique to external noise. Such analysis is also important from the point of view of practical applicability of this technique to an experimental analog system which would be exposed to inevitable external noise.

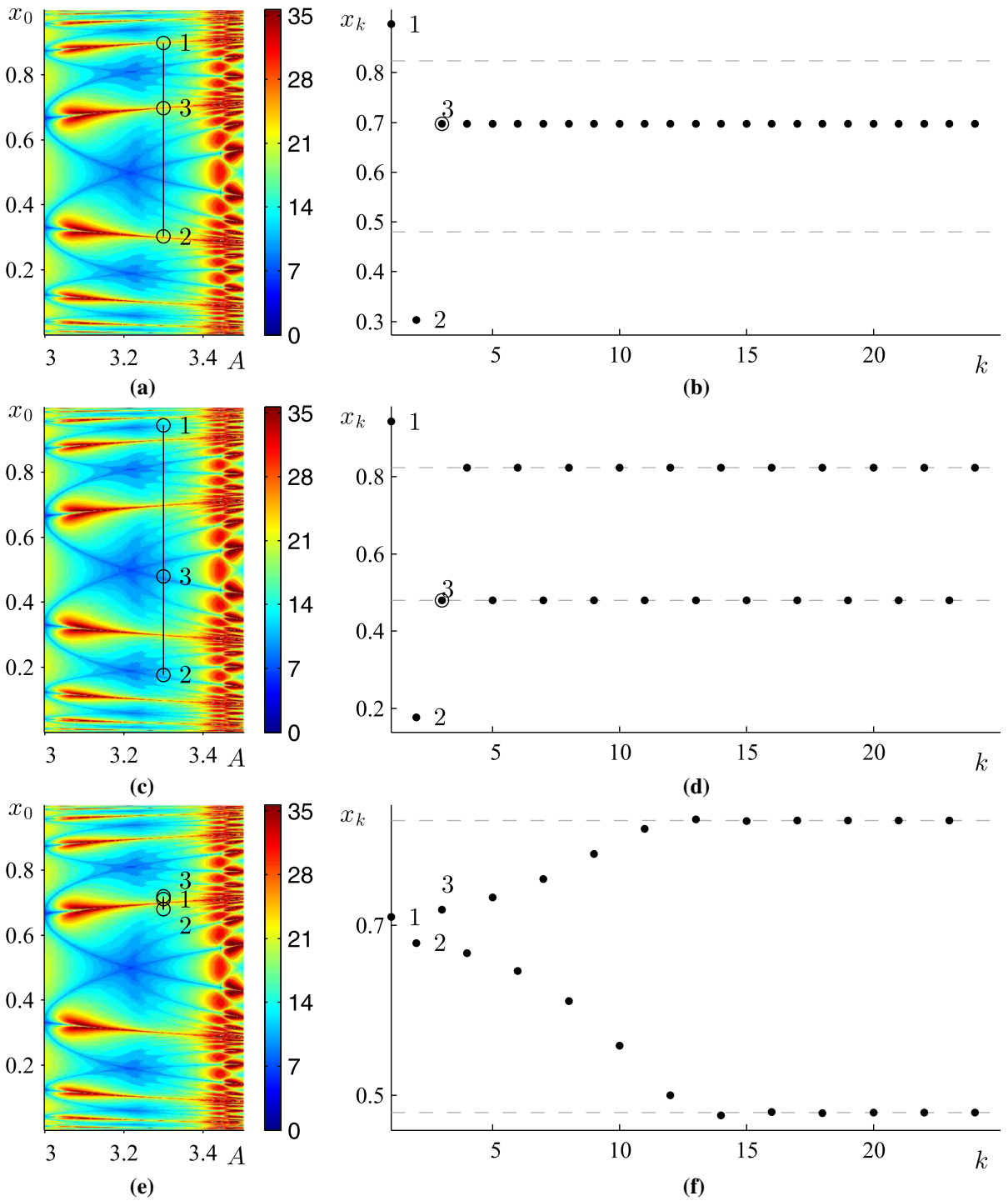

Fig. 10 Three different types of transient processes for the non-invertible logistic map $x_{n+1} = rx_n(1 - x_n)$. Parts **a** and **b** illustrate non-asymptotic convergence to the unstable period-1 repeller (the initial condition is located at the center of the second upper tulip in the pattern of H-ranks). Parts **c** and **d** illustrate non-asymptotic convergence to the stable period-2 attractor in two forward steps; parts **e** and **f** illustrate asymptotic convergence to the stable period-2 attractor. The parameter r is fixed to 3.3 in all computational experiments

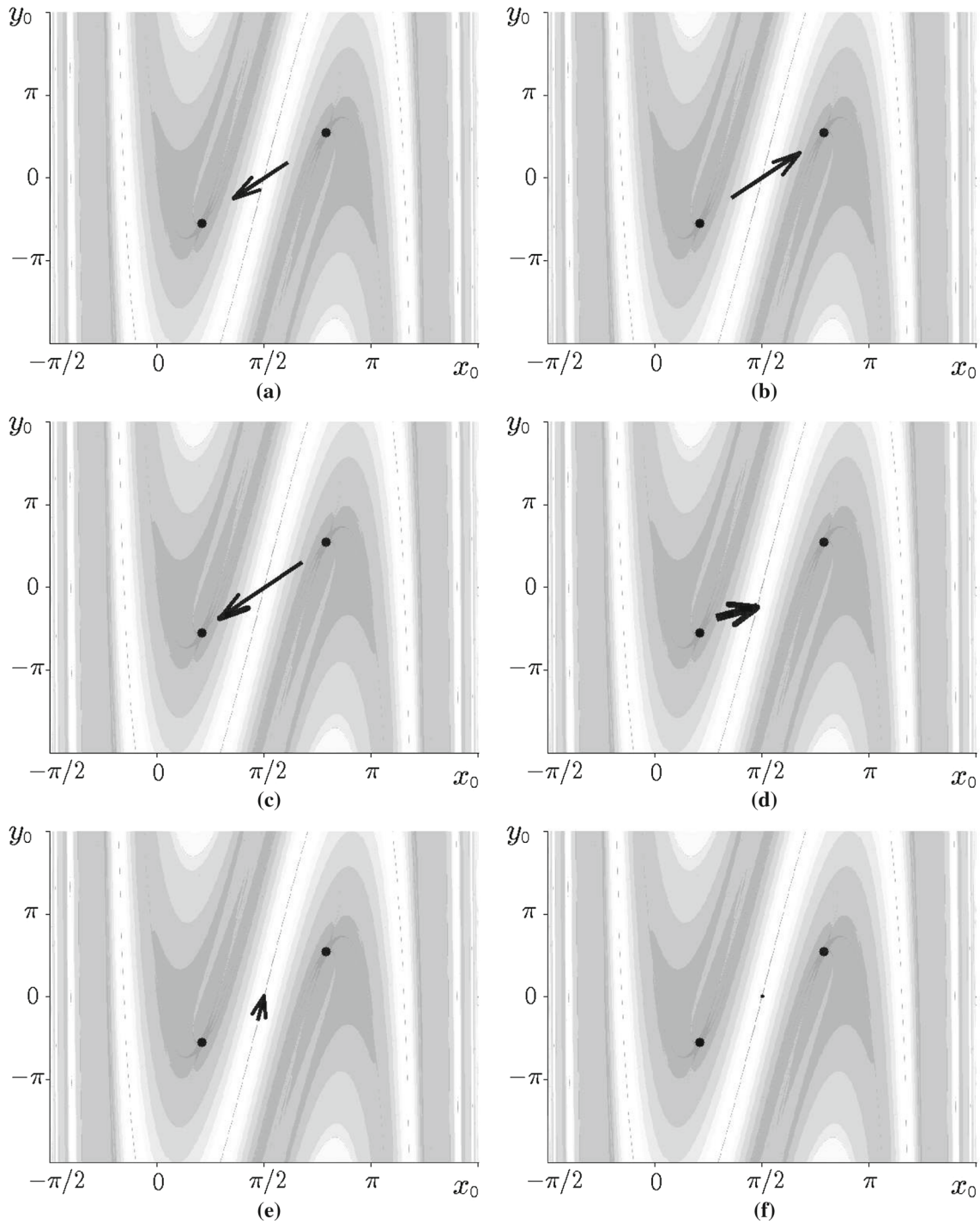

Fig. 11 The control strategy illustrated at $\alpha = 0.1$ and $\beta = 2.5$ (the grayscale pattern of H-ranks is shown in the background for clarity). *Thin black arrows* illustrate the evolution of the system without any control applied—the system approaches the stable period-2 regime (illustrated by two *thick black dots*) in parts (**a**), (**b**), and (**c**). The *thick arrow* in part (**d**) illustrates the control impulse which relocates the system onto a point on the pseudo-stable structure. The system converges to the period-1 regime in a finite number of steps as shown in parts (**e**) and (**f**) (no control is further required)

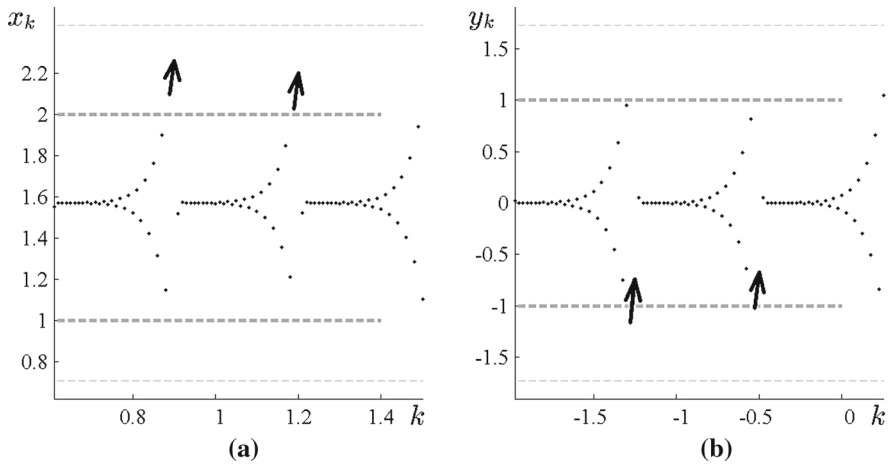

Fig. 12 The control strategy illustrated for the bouncer model—the evolution of x_k and y_k is shown in parts (**a**) and (**b**). *Thin dashed lines* stand for the stable period-2 attractor; *thick dashed lines* show the acceptable range for the deflection from the unstable period-1 repeller. *Thick arrows* denote the relocation of the system by a control pulse

Thus, the perturbed system reads

$$x_{n+1} = x_n + y_n + b\xi_n;$$
$$y_{n+1} = \alpha y_n + \beta \cos(x_n + y_n).$$

where ξ_n is Gaussian white noise with zero mean and a standard deviation equal to one; b is the noise intensity. We do perturb the time interval between the collisions; the velocity is perturbed automatically in the every subsequent collision.

Three computational experiments are performed at $b = 0.0001$, $b = 0.001$ and $b = 0.01$ (Fig. 13); 50 experiments are repeated from the same initial conditions as used in Fig. 8 parts b and c. Black dots in Fig. 13 correspond to unperturbed transient solutions (identical to ones illustrated in Fig. 8 parts b and c); gray dots correspond to 50 perturbed transients. It is clear that small external noise does not damage the temporary stabilization of the unstable orbit—though the resulting time interval when the transient solution stays in the surrounding of the unstable period-1 repeller is in average shorter compared to the unperturbed case. By the way, there exist particular transient solutions (Fig. 13) which stay longer in the surrounding of the repeller compared to the unperturbed system. That is an interesting phenomenon which could be explained by the fact that noise may change the stability of nonlinear systems [14]. In other words, a proper manipulation with particular realizations of the Gaussian noise may enable the design of efficient control strategies of unstable orbits. Nonetheless, we do leave these questions as a definite topic of future research.

7 Concluding remarks

Non-asymptotic convergence to unstable periodic orbits in non-invertible nonlinear maps is a well-known effect in nonlinear dynamics. But non-asymptotic convergence is not possible in completely invertible nonlinear maps (otherwise these maps cannot be invertible). This paper gives the computational proof of the fact that a pseudo-stable structure of non-asymptotic convergence to an unstable orbit may exist in a completely invertible discrete dynamical system.

A computational framework for the identification of this pseudo-stable structure attracting to the unstable period-1 repeller in the bouncer model is presented in this paper. The same framework is easily extendable for other completely invertible maps and more complex unstable periodic orbits. Our study was based on the bouncer system (Eq. 1)—but a complete computational analysis of the bouncing ball model remains a definite topic of future research.

The attraction of this pseudo-stable structure resembles non-asymptotic convergence to unstable periodic orbits in non-invertible nonlinear maps. But this attraction is only temporary since non-asymptotic convergence cannot exist in completely invertible maps. It is demonstrated that this pseudo-stable structure can be effectively exploited for temporary stabilization of unstable periodic orbits.

It is shown that the proposed technique for temporary stabilization of unstable periodic orbits in completely invertible maps is robust to external noise. It appears that particular realizations of the Gaussian

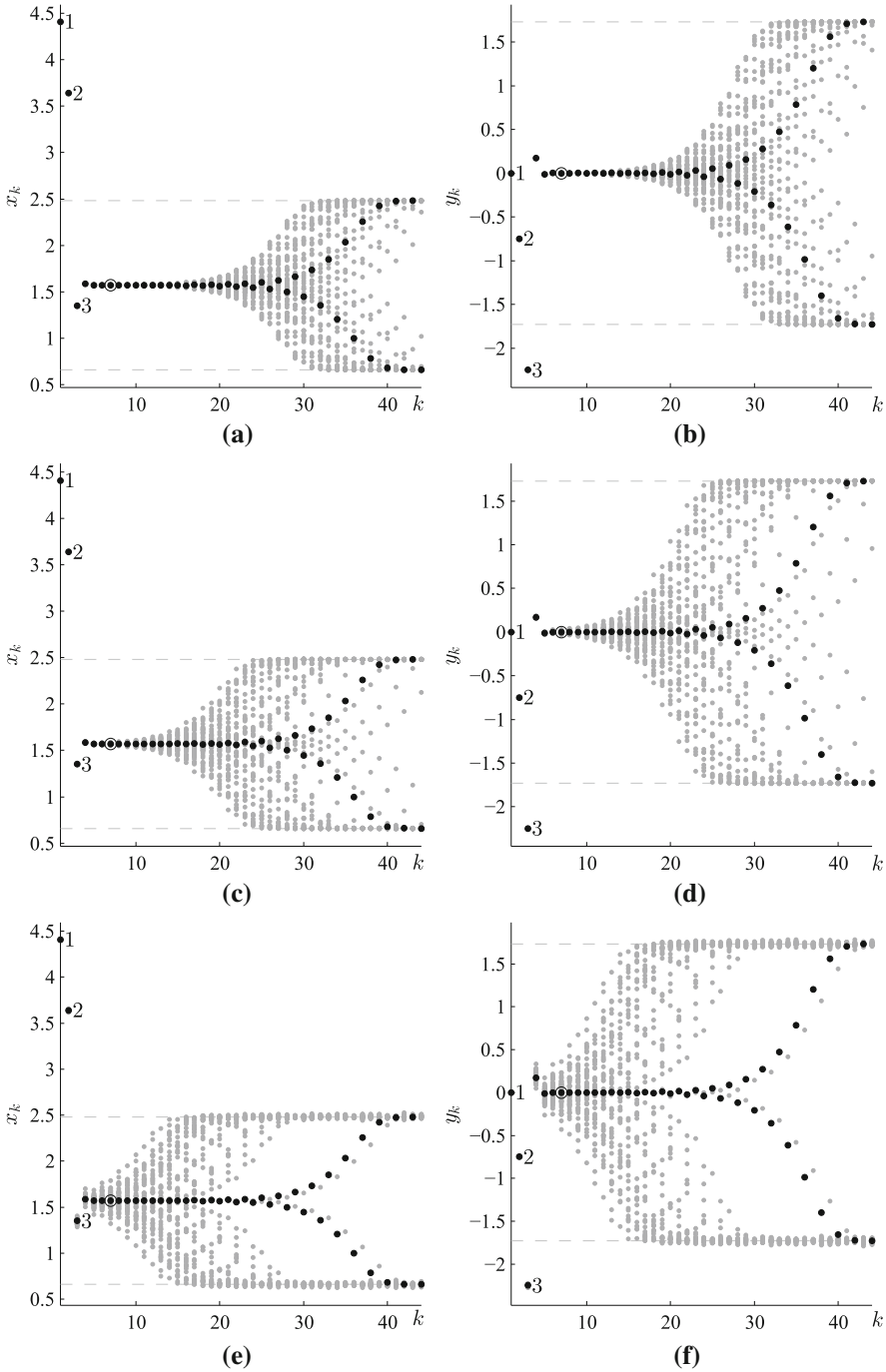

Fig. 13 The evolution of perturbed transient processes by Gaussian noise at: $b = 0.0001$ (parts **a** and **b**); $b = 0.001$ (parts (**c** and **d**); $b = 0.01$ (parts **e** and **f**). 50 perturbed transients are plotted as arrays of *gray dots*; the unperturbed transient—as a sequence of *black dots*

noise may extend the time interval when transient solutions stay in the surrounding of the unstable periodic orbit. This phenomenon could be explained by the fact that noise may change the stability of nonlinear systems—but the design of efficient control strategies based on external noise in completely invertible maps is left as a definite object of future research.

Acknowledgments Financial support from the Lithuanian Science Council under project No. MIP-100/2012 is acknowledged.

References

1. Broer, H.W., Osinga, H.M., Vegter, G.: Algorithms for computing normally hyperbolic invariant manifolds. Z. Angew. Math. Phys. **48**(3), 480–524 (1997)
2. Chirikov, B.V.: A universal instability of many-dimensional oscillator systems. Phys. Rep. **52**(5), 263–379 (1979)
3. Dellnitz, M., Hohmann, A.: A subdivision algorithm for the computation of unstable manifolds and global attractors. Numer. Math. **75**(3), 293–317 (1997)
4. Everson, R.: Chaotic dynamics of a bouncing ball. Phys. D: Nonlinear Phenom. **19**(3), 355–383 (1986)
5. Fermi, E.: On the origin of the cosmic radiation. Phys. Rev. **75**(8), 1169–1174 (1949)
6. Goodman, R.H., Wrbel, J.K.: High-order bisection method for computing invariant manifolds of two-dimensional maps. Int. J. Bifurc. Chaos **21**(7), 2017 (2011)
7. Guckenheimer, J., Holmes, P.J.: Nonlinear Oscillations, Dynamical Systems, and Bifurcations of Vector Fields. Springer, Berlin (1983)
8. Guo, Y., Luo, A.C.J.: Analytical predication of complex motion of a ball in a periodically shaken horizontal impact pair. J. Comput. Nonlinear Dyn. **7**(2), 021001–021009 (2011)
9. Hilborn, R.C.: Chaos and Non-linear Ddynamics. Oxford University Press, Norfolk (2000)
10. Hobson, D.: An efficient method for computing invariant manifolds for planar maps. J. Comput. Phys. **104**(1), 14–22 (1993)
11. Holmes, P.J.: The dynamics of repeated impacts with a sinusoidally vibrating table. J. Sound Vib. **84**(2), 173–189 (1982)
12. Hongler, M.O., Cartier, P., Flury, P.: Numerical study of a model of vibro-transporter. Phys. Lett. A **135**(2), 106–112 (1989)
13. Hongler, M.O., Figour, J.: Periodic versus chaotic dynamics in vibratory feeders. Helv. Phys. Acta **62**(1), 68–81 (1989)
14. Hutt, A.: Additive noise may change the stability of nonlinear systems. EPL **84**(3), 34003–34008 (2008)
15. Joseph, S.K., No, I.P.M., Sanjuán, M.A.F.: Effect of the phase on the dynamics of a perturbed bouncing ball system. Commun. Nonlinear Sci. Numer. Simulat. **17**(8), 3279–3286 (2012)
16. Kostelich, E.J., Yorke, J.A., Zhiping, Y.: Plotting stable manifolds: error estimates and noninvertible maps. Phys. D: Nonlinear Phenom. **93**(3–4), 210–222 (1996)
17. Kowalik, Z.J., Franaszek, M., Pierański, P.: Self-reanimating chaos in the bouncing-ball system. Phys. Rev. A **37**(10), 4016–4022 (1988)
18. Krauskopf, B., Osinga, H.: Growing 1D and quasi-2D unstable manifolds of maps. J. Comput. Phys. **146**(1), 404–419 (1998)
19. Landauskas, M., Ragulskis, M.: Clocking convergence to a stable limit cycle of a periodically driven nonlinear pendulum. Chaos **22**(3), 1054–1500 (2012)
20. Landauskas, M., Ragulskis, M.: Clocking convergence to Arnold tongues—the H-rank approach. AIP Conf. Proc. **1558**, 2457–2460 (2013)
21. Lichtenberg, A.J., Lieberman, M.A., Cohen, R.H.: Fermi acceleration revisited. Phys. D: Nonlinear Phenom. **1**(3), 291–305 (1980)
22. Lieberman, M.A., Lichtenberg, A.J.: Stochastic and adiabatic behavior of particles accelerated by periodic forces. Phys. Rev. A **5**(4), 1852–1866 (1972)
23. Luo, A.C., Han, R.P.: The dynamics of a bouncing ball with a sinusoidally vibrating table revisited. Nonlinear Dyn. **10**(1), 1–18 (1996)
24. Luo, A.C.J., Guo, Y.: Vibro-impact Dynamics. Wiley, Hoboken (2013)
25. Moore, G., Hubert, E.: Algorithms for constructing stable manifolds of stationary solutions. IMA J. Numer. Anal. **19**(3), 375–424 (1999)
26. Nusse, H.E., Yorke, J.A.: Dyn.: Numer. Explor. Springer, New York (1998)
27. Pierański, P., Mal/ecki, J.: Noisy precursors and resonant properties of the period-doubling modes in a nonlinear dynamical system. Phys. Rev. A **34**(1), 582–590 (1986)
28. Pustilnikov, L.D.: On Ulam's problem. Theor. Math. Phys. **57**, 1035 (1983)
29. Ragulskis, M., Navickas, Z.: The rank of a sequence as an indicator of chaos in discrete nonlinear dynamical systems. Commun. Nonlinear Sci. Numer. Simulat. **16**(7), 2894–2906 (2011)
30. Wiesenfeld, K., Tufillaro, N.B.: Suppression of period doubling in the dynamics of a bouncing ball. Phys. D: Nonlinear Phenom. **26**(1–3), 321–335 (1987)
31. Zaslavsky, G.: The simplest case of a strange attractor. Phys. Lett. A **69**(3), 145–147 (1978)